Smart Agricultural Technology 12 (2025) 101318

Contents lists available at ScienceDirect

Smart Agricultural Technology

journal homepage: www.journals.elsevier.com/smart-agricultural-technology

Extrinsic parameter calibration methods of sensors present in a robot tractor

Jere Knuutinen [a,b,*], Juha Backman [b,a], Raimo Linkolehto [b], Arto Visala [a]

[a] Department of Electrical Engineering and Automation, Aalto University, Espoo, 02150, Finland
[b] Farming Technologies, Natural Resources Institute Finland (Luke), Helsinki, 00790, Finland

ARTICLE INFO

Keywords:
Extrinsic calibration
3D LiDAR
Camera
GNSS/IMU
Cross-validation

ABSTRACT

To achieve large-scale deployment of autonomous agricultural machines, a reliable and accurate perception system must be developed. Often, autonomous machines use and require data from several sensors to work optimally and safely. Therefore, accurate extrinsic parameter calibration between various sensors is one of the first prerequisites.

This paper equips an actual robot tractor with two LiDAR sensors, a stereo camera, and a GNSS/IMU unit and it investigates different extrinsic calibration methods between them in the agricultural environment. The extrinsic calibration method between the LiDAR sensors utilizes extracted planar structures from point clouds. In the case of the LiDAR and the GNSS/IMU unit, two calibration methods are developed. The first method utilizes LiDAR point cloud features, whereas the second method uses sensor motion estimates. In turn, the LiDARs and the camera are extrinsically calibrated using a traditional checkerboard method. The results with the actual robot tractor show that the methods achieve correct and consistent calibration results in the agricultural environment. The optimization functionality of the LiDAR-to-LiDAR calibration method was validated using simulation. In addition, the actual results are validated by cross-validation by calculating extrinsic parameters between LiDAR sensors using the other methods mentioned above. The average standard deviation of the results is 0.3189° for rotation and 0.0491 m for translation parameters. In addition, a visual examination of the results strengthens this conclusion.

1. Introduction

Agriculture has a major effect on the world economy. Its share being 4% of the global gross domestic product [1]. Historically, the agricultural field has demanded and relied on manual work and conventional production methods. However, in recent decades, precision farming has begun to replace traditional practices to some extent. In precision farming, the aim is to improve the production output of agriculture, but so that the environmental effect decreases [2]. In addition, robotics has also attracted increasing interest in recent years. An example of this is the concept of a robot tractor.

Agricultural environments are typically complex and unstructured [3][4]. Because of these factors, among the first requirements for the widespread adoption of autonomous agricultural machinery is the construction of a robust perception system. When the perception system is being developed, it is usually reasonable to fuse measurements from different sensors to obtain a more complete picture of the environment. In order to fuse data from different sensors effectively, they have to be calibrated extrinsically. In the extrinsic parameter calibration, the rotation and translation parameters between the sensor frames have to be found.

Previous studies have proposed several different approaches to the problem of extrinsic parameter calibration depending on, for example, the required level of automation, sensor types, or the structure of the environment. For example, methods that require artificial calibration targets such as checkerboards are often utilized. A planar board with reflective tape was used to calibrate extrinsic parameters between LiDARs in [5]. The board was first detected from the point clouds, and subsequently the authors formulated an optimization problem to solve rotation. Furthermore, the translation was solved utilizing intersection points of the planes. Zhou et al. [6] showed an approach in which extrinsic parameters were calculated between the LiDAR and the camera using the checkerboard. The study utilized both the plane and the 3D line

* Corresponding author at: Department of Electrical Engineering and Automation, Aalto University, Espoo, 02150, Finland.
E-mail addresses: Jere.Knuutinen@aalto.fi (J. Knuutinen), Juha.Backman@luke.fi (J. Backman), Raimo.Linkolehto@luke.fi (R. Linkolehto), Arto.Visala@aalto.fi (A. Visala).

https://doi.org/10.1016/j.atech.2025.101318
Received 11 June 2025; Received in revised form 12 August 2025; Accepted 12 August 2025

Available online 25 August 2025

correspondences. The authors stated that it is achievable to determine correct extrinsic parameters using only one checkerboard configuration. In [7], an extrinsic calibration method for camera and LiDAR setups was shown. The method used a custom calibration target that contained circular holes and ArUco markers.

Another class of methods utilizes environmental structures, such as plane structures from the environment, when calibrating extrinsic parameters. In [8] planar objects from the environment were used to calibrate the LiDAR sensors. The proposed method utilized a region-growing-based segmentation and MLESAC to get planar structures from point clouds. The method was separated into two parts. At first, the initial estimation for the parameters was calculated using the Kabsch algorithm. After that, the estimates were improved by minimizing a nonlinear cost function. Jiao et al. [9] showed a alike method for the LiDAR-to-LiDAR calibration problem. In the proposed method, the planes were extracted using Random Sample Consensus (RANSAC), and the initial estimate was determined using the Kabsch algorithm and the plane intersections. Furthermore, the estimate was improved using nonlinear optimization. Also in [10], the plane structures were utilized. The proposed approach used a polar view transform to find features needed to find corresponding planes from point clouds.

An alternative group of methods uses sensor motion estimates in extrinsic parameter calibration. The motion-based calibration approaches currently common in autonomous vehicle applications are usually founded on the same fundamentals as the hand-eye calibration methods that have been researched since the 1980s [11]. A common application is to apply motion-based calibration between two LiDARs. In [12] iterative closest point (ICP) method was used to generate motion estimates of the LiDAR sensors. After that, the study developed a nonlinear manifold optimization method based on sensor motion. The initial estimates for the extrinsic parameters between LiDAR sensors were determined using the motion-based approach in [13]. The developed method included two steps: first pitch and roll angles were calculated, followed by the yaw rotation and the x and y translations. The motion-based part of the method did not consider the z-axis translation. In [14] the calibration of extrinsics between the camera and the LiDAR was conducted using the motion-based approach. The developed method separated the estimation into initialization and iteration.

The motion-based calibration approach is also studied between the LiDAR and the GNSS/IMU unit. The method presented in [15] was used in the study by Geiger et al. [16]. In [17] a two-step calibration process between a LiDAR and GPS/IMU was shown. In the first step, the proposed method calculates rotation and translation separately. It also utilizes loop closure techniques. In the second step, it calculates a new lidar odometry using scan-to-map matching. The method was not capable to estimate the z-axis accurately. The method presented in [18] utilized different kinds of trajectories to determine rotation and translation parameters. Trajectories with larger profile were used in the case of rotation parameters. In turn, trajectories with a small profile were used in the case of translation.

The previous literature also contains studies where the GNSS/IMU and LiDAR are calibrated using a point-cloud-based approach. In [19] a GNSS/INS and a LiDAR were extrinsically calibrated in a two-step manner. First, the paper used plane features. After that, refinement was performed using octree-based optimization. The calibration of the translation parameter of the z axis was based on fiducial points. In [20] point cloud-based extrinsic calibration was studied between a solid-state LiDAR and a GNSS/INS unit. The paper also included motion-based constraints to the optimization. In [21] the same set of sensors was calibrated extrinsically. The paper utilized the perturbation model of Lie algebras.

The main objective of this paper is to study extrinsic parameter calibration methods in the case of a robot tractor in an agricultural environment. The aim is not only to obtain accurate extrinsic parameters between the sensors but also to study the methods in terms of how well they are suited for automatic calibration. More precisely, the paper investigates extrinsic calibration methods between different sensors and configurations. The robot tractor is equipped with two Velodyne VLP-16 LiDARs, a Stereolabs ZED2 stereo camera, and a GNSS/IMU unit. The first developed calibration method uses detected planar structures from the environment. This method is used to calibrate extrinsic parameters between two LiDAR sensors. In turn, both point-cloud-based and motion-based calibration methods are studied between the GNSS/IMU unit and LiDAR calibration. Finally, the extrinsic parameters are obtained between the camera and the LiDARs using the traditional checkerboard method. Furthermore, the results are cross-validated by estimating the LiDAR-to-LiDAR extrinsics parameters using different methods. To the authors' knowledge, there have been a limited number of studies of extrinsic calibration methods in this particular context.

2. Materials and methods

2.1. Research platform, sensor mounting and data acquisition

This study uses commercial tractor from Valtra to conduct needed experiments. Fig. 1 (a) shows the tractor. Furthermore, Fig. 1 (b) shows the sensor frames. Modifications to the tractor have been made that enable it to be used as a robot. Before this study, the tractor already included an RTK-GNSS/IMU unit, a Valtra guide auto-steering module, and ISOBUS features. A comprehensive overview of this particular tractor can be found in [22]. In this study, two VLP-16 LiDAR sensors and the ZED2 stereo camera are mounted on the tractor.

The VLP-16 LiDAR sensor only has a 30-degree vertical field of view and 16 scan lines. Therefore, the LiDAR sensors were mounted on both sides of the tractor's roof and were mounted tilted forward and to the side. If the sensors were placed horizontally, the first points would be distant. The ZED2 stereo camera was mounted on the roof of the tractor between the LiDARs. LiDAR data were collected using Velodyne's ROS2 driver and ZED2 data were collected using the ZED ROS2 wrapper. Both sensors were sampled at 10 Hz. In addition, data from the GNSS/IMU unit were acquired at 10 Hz.

2.2. LiDAR-to-LiDAR extrinsic calibration using environmental structures

The LiDAR-to-LiDAR extrinsic calibration method is founded on planes extracted from the environment. At first, region-growing segmentation is used to find planar surfaces from the LiDAR point clouds. In contrast, the actual plane parameters are obtained using the M-estimator SAmple Consensus (MSAC) algorithm. Note that all the planes do not have to be extracted from one position, but multiple different positions can be utilized. In the next phase, the corresponding planes are found. In the third step, the optimization problem is formulated as a plane-to-plane registration problem. Fig. 2 shows a flow chart of the method. The next sections elaborate on the method.

2.2.1. Plane extraction and matching

Planar structures in point clouds are found using region growing segmentation. Furthermore, the actual parameters of the planes are obtained by utilizing MSAC-based estimation. In more exact terms, the needed plane parameters are a normal vector and a distance from the origin.

The idea behind the plane extraction was presented in [8]. The underlying concept of region-growing segmentation is to use the smoothness constraint to locate planar objects from point clouds [23]. For a chosen set of points in the point cloud, smoothness can be detected using normal vectors [23]. Point cloud data points can be considered to be members of the same planar surface if the angle between the normal vectors is small [24]. The region is increased by iterations until the conditions no longer hold. In the region growing a smoothness threshold of 2 degrees is used. After segmentation, the obtained clusters can still contain outliers. Because of this, filtering based on a principal component analysis is utilized. Filtering is done as follows: if λ_1, λ_2, and

(a) (b)

Fig. 1. (a) Valta N135D tractor that is used as the research platform in this study. (b) shows the sensor frames. The red arrow is the x-axis, the green arrow is the y-axis and the blue arrow is the z-axis.

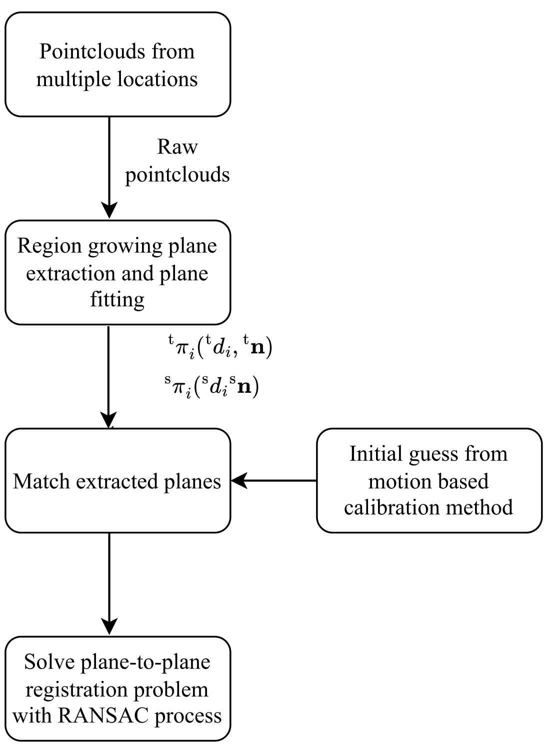

Fig. 2. Flowchart of LiDAR-to-LiDAR extrinsic calibration method. First, raw point clouds are fed into region-growing-based plane extraction and plane fitting. After that, planes are matched. Also, an initial guess is provided to make the plane-matching process more accurate. Finally, the plane-to-plane registration problem is solved.

λ_3 are the eigenvalues of a planar surface covariance matrix. Then it should hold that $\lambda_1 \gg \lambda_3$ and $\lambda_2 \gg \lambda_3$ if the surface is planar shaped. In addition, λ_3 should be smaller than some threshold τ_{thr}. The planar object should also have more than N_{thr} data points. Once this is done, MSAC-based plane fitting is used to obtain plane parameters. In this paper the following parameter values are used $\tau_{\text{thr}} = 0.07$, $N_{\text{thr}} = 200$ and MSAC with iterations of 1000 and max distance of 0.01 m.

Once the planar structures as well as the plane parameters have been obtained, the corresponding planes need to be determined between two point clouds. This is typically known to be a problem of data association. In this work a method utilizes an initial transformation matrix obtained using a method introduced in section 2.3.2, the plane parameters, and linear assignment method called *matchpairs* provided by MATLAB. The normals of the planes and the closest points are utilized to form the required cost for the *matchpairs* method. The plane normals are used to calculate the difference between the normals, whereas closest points are utilized to add cost based on distance. In turn, the initial transformation is used to make the matching process more accurate.

2.2.2. *Finding optimal extrinsic parameters using plane-to-plane registration*

After region growing segmentation, plane parameter estimation and plane matching, the extrinsic parameters can be estimated. In order to determine these, a plane-to-plane registration problem is solved. A closed-form solution can be used to solve this, as reported in [25] and [26]. In addition, the rotation and translation parameters can be solved separately. As mentioned, the normal vector and the distance from the origin can be used to describe the planar object. For this reason, the corresponding normal vectors are presented to be $\mathbf{n}_i^{\text{Left}}$ and $\mathbf{n}_i^{\text{Right}}$ and the corresponding distances d_i^{Left} and d_i^{Right}. Therefore, the rotation parameters are obtained by minimizing the following cost:

$$\sum_{i=1}^{N} ||\mathbf{R}_{\text{Right}}^{\text{Left}} \mathbf{n}_i^{\text{Right}} - \mathbf{n}_i^{\text{Left}}||^2, \tag{1}$$

where $\mathbf{R}_{\text{Right}}^{\text{Left}}$ is the rotation matrix between the right LiDAR frame and the left LiDAR frame. Using Singular Value Decomposition (SVD) the rotation can be determined. At first, correlation matrix $\mathbf{H}$ is built:

$$\mathbf{H} = \sum_{i=1}^{N} \mathbf{n}_i^{\text{left}\top} \mathbf{n}_i^{\text{Right}}. \tag{2}$$

Then, the rotation matrix estimate can be calculated with

$$\mathbf{R} = \mathbf{V}\begin{bmatrix} 1 & & \\ & 1 & \\ & & \det(\mathbf{V}\mathbf{U}^{\mathrm{T}}) \end{bmatrix}\mathbf{U}^{\mathrm{T}}, \tag{3}$$

where $\mathbf{V}$ and $\mathbf{U}$ are given by SVD ($\mathbf{H} = \mathbf{USV}^{\mathbf{T}}$). The translation vector $\mathbf{t}$ can be determined by minimizing the following:

$$\sum_{i=1}^{N}(\mathbf{n}_i^{\mathrm{Left}}\mathbf{t}_i - (d_i^{\mathrm{Right}} - d_i^{\mathrm{Left}}))^2. \tag{4}$$

The resulting equation from equation (4) has the following form:

$$\begin{bmatrix} \mathbf{n}_1^{\mathrm{Left}} \\ \vdots \\ \mathbf{n}_N^{\mathrm{Left}} \end{bmatrix}\mathbf{t} = \begin{bmatrix} d_1^{\mathrm{Right}} - d_1^{\mathrm{Left}} \\ \vdots \\ d_N^{\mathrm{Right}} - d_N^{\mathrm{Left}} \end{bmatrix}, \tag{5}$$

because plane matches can contain wrong associations, the RANSAC-based method is used to filter outliers. The first metric that is used is a point-to-plane distance. This can be calculated with the following equation

$$d_i^{\perp} = ||\mathbf{n}^{\mathrm{Left}} \cdot (\mathbf{T}_{\mathrm{Right}}^{\mathrm{Left}}\mathbf{p}^{\mathrm{Right}} - \mathbf{p}^{\mathrm{Left}})||^2. \tag{6}$$

In equation (6) $\mathbf{T}_{\mathrm{Right}}^{\mathrm{Left}}$ is a 4x4 transformation matrix that has the rotation and translation parameters and where $\mathbf{p}^{\mathrm{Right}}$ and $\mathbf{p}^{\mathrm{left}}$ are points on the right and left frame planes, respectively. Another metric that is utilized is the angle between the left plane normal and the rotated right plane normal. This can be calculated with the following:

$$\theta_{\mathrm{normals}} = \arccos\left(\frac{\mathbf{n}^{\mathrm{left}\top} \cdot (\mathbf{R}_{\mathrm{Right}}^{\mathrm{left}}\mathbf{n}^{\mathrm{Right}})}{||\mathbf{n}^{\mathrm{left}}||\,||\mathbf{n}^{\mathrm{Right}}||}\right). \tag{7}$$

In addition, the transformation has to be valid, meaning that the determinant has to be 1, and the number of inliers has to be higher than the predefined threshold.

2.3. Extrinsic calibration between the LiDAR and the GNSS/IMU

This section provides two approaches to estimate extrinsic parameters between the LiDAR and the GNSS/IMU. The first method is based on LiDAR point clouds. The second one is based on LiDAR and GNSS/IMU motion.

2.3.1. Extrinsic calibration using point clouds

The point cloud-based extrinsic calibration method is based on GNSS/IMU position and orientation data and the separation of cylindrical objects from the point cloud at different times. The method can also be extended to include other features already found in the environment. The calibration problem can be solved with the following equation.

$$\mathbf{X}_{\mathrm{LiDAR}}^{\mathrm{GNSS/IMU}} = \underset{\mathbf{X}_{\mathrm{LiDAR}}^{\mathrm{GNSS/IMU}} \in \mathbf{SE}(3)}{\arg\min} \sum_{i=1}^{N}\sum_{j=1}^{N} ||\mathbf{T}(t_i)_{\mathrm{GNSS/IMU}}^{\mathrm{Global}}\mathbf{X}_{\mathrm{LiDAR}}^{\mathrm{GNSS/IMU}}\mathbf{p}(t_i)^{\mathrm{LiDAR}} - \mathbf{T}(t_j)_{\mathrm{GNSS/IMU}}^{\mathrm{Global}}\mathbf{X}_{\mathrm{LiDAR}}^{\mathrm{GNSS/IMU}}\mathbf{p}(t_j)^{\mathrm{LiDAR}}||^2, \tag{8}$$

where $\mathbf{X}_{\mathrm{LiDAR}}^{\mathrm{GNSS/IMU}}$ is the pose of the LiDAR frame measured from the GNSS/IMU frame. In turn, $\mathbf{T}(t_i)_{\mathrm{GNSS/IMU}}^{\mathrm{Global}}$ is the pose of the GNSS/IMU frame measured from the global frame at time t. Moreover $\mathbf{p}(t)^{\mathrm{LiDAR}}$ is the cylinder point extracted in the LiDAR frame at time t. Equation (8) implies that two corresponding cylinder points from different time instances are rotated and translated to a global frame and that the extracted points should have the same location in the global frame.

The cylinder is extracted from the point cloud by clustering the input point cloud by finding the nearest neighbors within a certain range. After that, the cylinder model is fitted to the clustered data. Because the LiDAR point cloud may not contain all the points on the cylinder, the center point cannot be used. Instead, the point between the cylinder and the ground is used. This point is obtained by projecting the calculated center point onto the extracted ground plane.

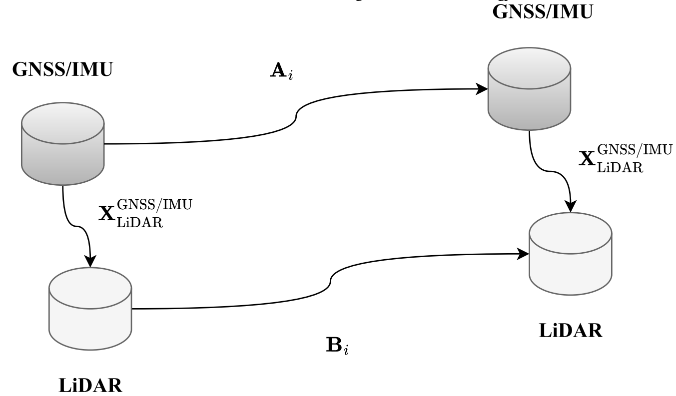

Fig. 3. The main concept of the motion-based calibration.

2.3.2. LiDAR to GNSS/IMU unit extrinsic calibration using sensor motion

Extrinsic calibration between the LiDAR and the GNSS/IMU unit can also be performed using a motion-based approach. This problem can be formulated as follows.

$$\mathbf{A}\mathbf{X}_{\mathrm{LiDAR}}^{\mathrm{GNSS/IMU}} = \mathbf{X}_{\mathrm{LiDAR}}^{\mathrm{GNSS/IMU}}\mathbf{B}. \tag{9}$$

In equation (9), $\mathbf{A}$ and $\mathbf{B}$ are poses of the sensors A and B between two timestamps t_i and t_{i+1}, respectively. As mentioned in [27], the pose estimates do not have to be consecutive. Instead, the reference pose can be the latest nth pose. Framing the problem in this style can reduce noise but choosing too large n can cause drift in the pose estimates [27]. In Fig. 3 main idea of the motion-based calibration is shown.

2.3.3. Sensor motion estimation and time offset estimation

As the equation (9) shows, the pose estimates of the sensor are required in the calibration. Therefore, it is necessary to be able to estimate the sensor's motion. In this paper, the Direct LiDAR Odometry method (DLO) [28] is used to obtain motion estimates for LiDARs. The motion estimate for the GNSS/IMU unit is determined by merging position values from the RTK-GNSS data and IMU angles. Furthermore, the latitude and longitude coordinates given by the GNSS unit are converted into local coordinates, and the GNSS/IMU poses are formed with respect to the first pose.

Cross-correlation is used to determine the possible time offset between the sensors. Cross-correlation can be utilized to determine the similarity of two signals. In this case, it can be used to calculate the time-offset of the motion estimates. The following equation is used to calculate the cross correlation:

$$r(l) = \sum_{i=-\infty}^{\infty} x(i)y(i-l), l = 0, \pm 1, \pm 2, \ldots \tag{10}$$

where x and y are two signals and the index l is the time shift parameter. In this paper angular velocities are used as signals since they are independent of the reference frame.

2.3.4. Motion based calibration

The central idea of the optimization method was given in [12]. The optimization problem can be derived from Equation (9) which results in the following:

$$\hat{\mathbf{X}}_{\mathrm{LiDAR}}^{\mathrm{GNSS/IMU}} = \underset{\mathbf{X} \in \mathbf{SE}(3)}{\arg\min} \sum_{i=1}^{N} ||\mathbf{A}_i\mathbf{X}_{\mathrm{LiDAR}}^{\mathrm{GNSS/IMU}}\mathbf{B}_i^{-1} - \mathbf{X}_{\mathrm{LiDAR}}^{\mathrm{GNSS/IMU}}||^2, \tag{11}$$

where $\mathbf{X}_{\mathrm{LiDAR}}^{\mathrm{GNSS/IMU}}$ is the pose (extrinsic parameters) of the LiDAR measured from the GNSS/IMU frame and where $\mathbf{B}_i$ and $\mathbf{A}_i$ are relative

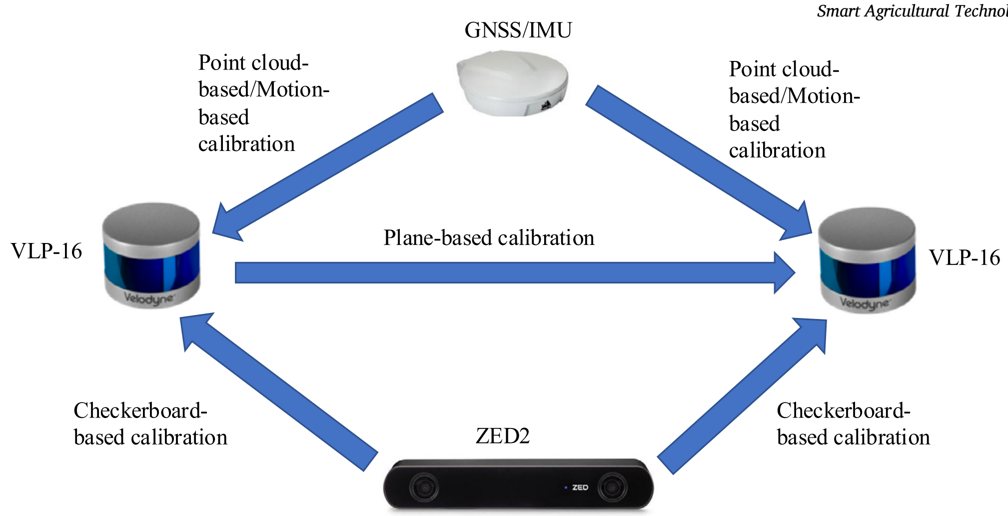

Fig. 4. Cross validation method used in this study. Besides directly obtaining LiDAR-to-LiDAR transformation using the developed plane-based calibration method, the transformation can also be obtained using the results obtained between the GNSS/IMU and the LiDARs and the camera and the LiDARs.

motion estimates between two timestamps. In practice, the cost is calculated as follow

$$\mathbf{M}_i = \mathbf{A}_i \mathbf{X}_{\text{LiDAR}}^{\text{GNSS/IMU}} \mathbf{B}_i^{-1} - \mathbf{X}_{\text{LiDAR}}^{\text{GNSS/IMU}} \tag{12}$$

$$J = \sum_{i=1}^{N} \mathrm{Tr}(\mathbf{M}_i \mathbf{M}_i^{\mathrm{T}}). \tag{13}$$

In equation (13) J is the total cost and Tr is the trace operator. Optimization is carried out subject to $\mathbf{X}_{\text{LiDAR}}^{\text{GNSS/IMU}} \in \mathbf{SE}(3)$ where $\mathbf{SE}(3)$ denotes the special euclidean group. Manopt toolbox for MATLAB is used to solve the optimization problem [29].

2.4. LiDAR-to-camera extrinsic calibration

The calibration of the camera-to-LiDAR transformation is based on the closed-source implementation of the MATLAB LiDAR toolbox [30]. When calibrating perception sensors with known calibration target, the LiDAR and the camera need to share the field of view. Furthermore, the implementation provided by the MATLAB locates the checkerboard corners from both the image data and point cloud data. Based on the corner points, the method calculates the transformation between the sensor frames. The camera intrinsics are known during the calibration.

2.5. Cross validation

To verify the correct functioning of the methods, cross-validation is used. The LiDAR-to-LiDAR transformation can be estimated using all the methods presented in the previous sections. First of all, the LiDAR-to-LiDAR extrinsics can be determined using the presented plane-based approach. The LiDAR-to-LiDAR transformation can also be obtained using the calibration results between the GNSS/IMU unit and the LiDARs, as well as by utilizing the results between the camera and the LiDARs. For example, if we know the extrinsic between the GNSS/IMU unit and LIDAR 1 ($\mathbf{X}_{\text{LiDAR1}}^{\text{GNSS/IMU}}$) as well as the extrinsics between the GNSS/IMU unit and the LiDAR 2 ($\mathbf{X}_{\text{LiDAR2}}^{\text{GNSS/IMU}}$). The pose of the LiDAR 2 frame measured from the LiDAR 1 frame can be calculated with

$$\mathbf{X}_{\text{LiDAR2}}^{\text{LiDAR1}} = (\mathbf{X}_{\text{LiDAR1}}^{\text{GNSS/IMU}})^{-1} \mathbf{X}_{\text{LiDAR2}}^{\text{GNSS/IMU}}. \tag{14}$$

The same logic can also be applied to the LiDAR and the camera. Fig. 4 summarizes the cross-validation method used in this paper.

Table 1
Results obtained from simulation environment. The ground truth and the estimated extrinsic parameter as well as the absolute error between the corresponding parameters are shown.

Parameter	Ground truth	Estimated value	Absolute error
t_x (m)	-0.3643	-0.3768	0.0126
t_y (m)	-1.3074	-1.3124	0.0049
t_z (m)	-0.3974	-0.4001	0.0027
ψ (°)	-42.2337	-42.3000	0.0663
θ (°)	-4.7546	-4.7984	0.0438
ϕ (°)	19.1840	19.2427	0.0587

3. Results

In this section, the extrinsic calibration results are presented. The section presents the results obtained between the LiDAR sensors when the plane-based calibration method is used. This calibration method is tested in the simulation environment as well as in the real calibration case. After that, the proposed motion-based calibration method is also being tested between LiDARs. Subsequently, the section shows the results between GNSS/IMU and LiDAR calibration when both the point-cloud-based method and the motion-based method are used. Finally, the results between the camera and the LiDAR are shown.

3.1. Results from LiDAR-to-LiDAR extrinsic calibration

3.1.1. Simulation results from plane-based calibration between LiDAR and LiDAR

ROS Gazebo environment enables simulation of VLP-16 LiDARs [31]. Therefore, the plane-based calibration method was examined in simulation. The created simulation environment contained two walls and a flat ground. This enabled the optimization functionality of the method to be tested. However, plane matching can not be tested as described in section 2.2 since the initial transformation is not available in simulation from the motion-based calibration method. The simulation environment also enables comparison between ground truth parameters and estimated parameters.

Both the ground truth and the estimated parameters from the simulation test are shown in Table 1. In addition, an absolute error between values is shown in the table. In the table, the translation parameters (t_x, t_y, t_z) are expressed in meters and the rotation parameters (ψ, θ, ϕ) are expressed in degrees using Euler angles. The same format is used throughout the study.

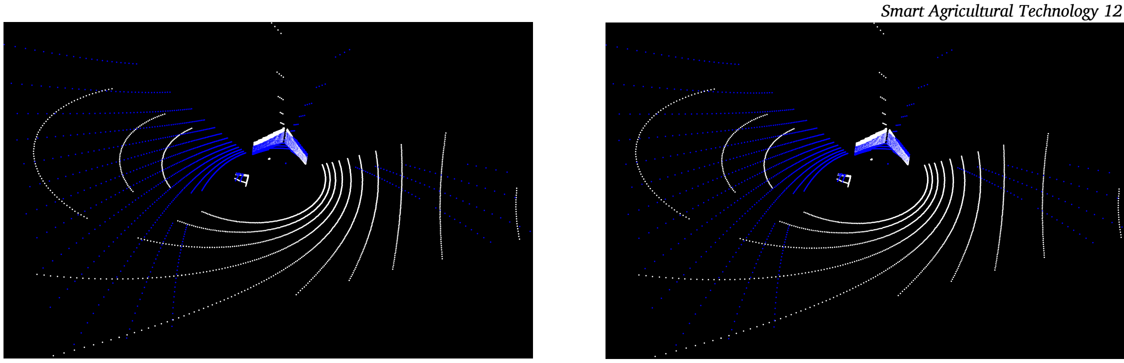

(a) Ground truth result (b) Calibration result

Fig. 5. Simulation results. (a) shows calibrated point clouds using the ground truth values. (b) shows calibrated point clouds using the estimated values.

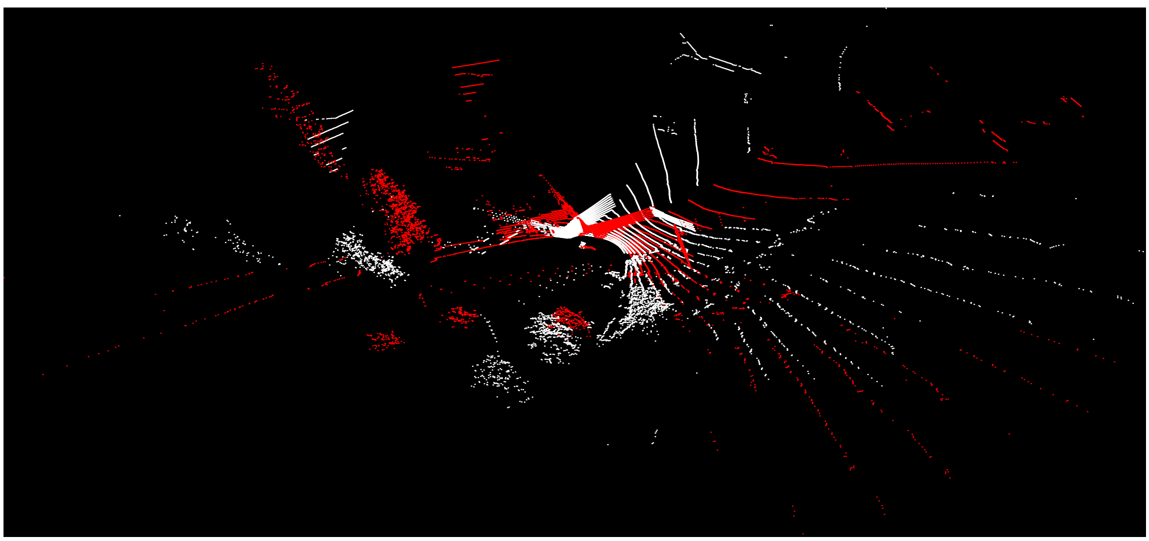

Fig. 6. Uncalibrated point clouds.

Table 2
Extrinsic parameter results between the left LiDAR and the right LiDAR when the plane-based calibration method presented in the section 2.2 is used.

Parameter	Value
t_x (m)	-0.35
t_y (m)	-1.30
t_z (m)	-0.14
ψ (°)	-26.74
θ (°)	5.05
ϕ (°)	11.02

Table 3
Extrinsic parameters obtained between the left LiDAR and the right LiDAR when the motion-based method presented in the section 2.3.2 is used.

Parameter	Value
t_x (m)	-0.24
t_y (m)	-1.24
t_z (m)	-0.21
ψ (°)	-28.71
θ (°)	4.75
ϕ (°)	6.03

The simulation results can be seen from Fig. 5. Fig. 5 (a) shows the calibration result when the ground truth parameters are utilized, whereas Fig. 5 (b) shows the calibrated point clouds when the estimated values are used.

3.1.2. Results from plane-based calibration between LiDAR and LiDAR

In this section, the plane-based calibration results are presented when it is used in the real calibration case. Because ground truth values are not available, Table 2 shows the estimated values for the extrinsic parameters obtained when using the plane-based method. In addition, a visual presentation of the results is shown. In Fig. 6 uncalibrated point clouds are shown. Following this, the calibrated point clouds can be seen in Fig. 7 when the estimated values are used.

3.1.3. Results from motion-based calibration between LiDAR and LiDAR

The LiDARs were also calibrated using motion-based approach introduced in Section 2.3.2. This enables further testing of the motion-based calibration method and provides confirmation of the results obtained in the previous section. It also shows that motion-based calibration can be utilized with different sensor types. Table 3 shows the estimated numerical values for the translation and rotation parameters that are obtained when the motion of LiDAR is estimated using merged point clouds from both LiDARs. The results can be seen in Fig. 8. In Fig. 8 the same scene as in Fig. 7 is shown.

3.2. Results from extrinsic calibration between the GNSS/IMU unit and LiDAR

This section shows the extrinsic calibration results between the GNSS/IMU unit and the LiDAR sensors. The section shows the results

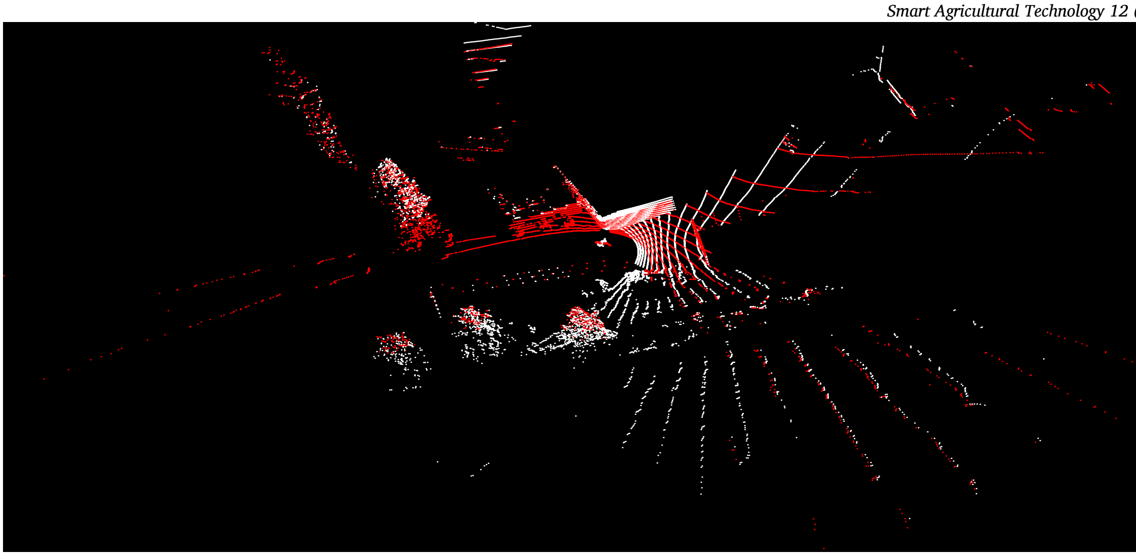

Fig. 7. Calibrated point clouds when the parameters shown in the Table 2 are used.

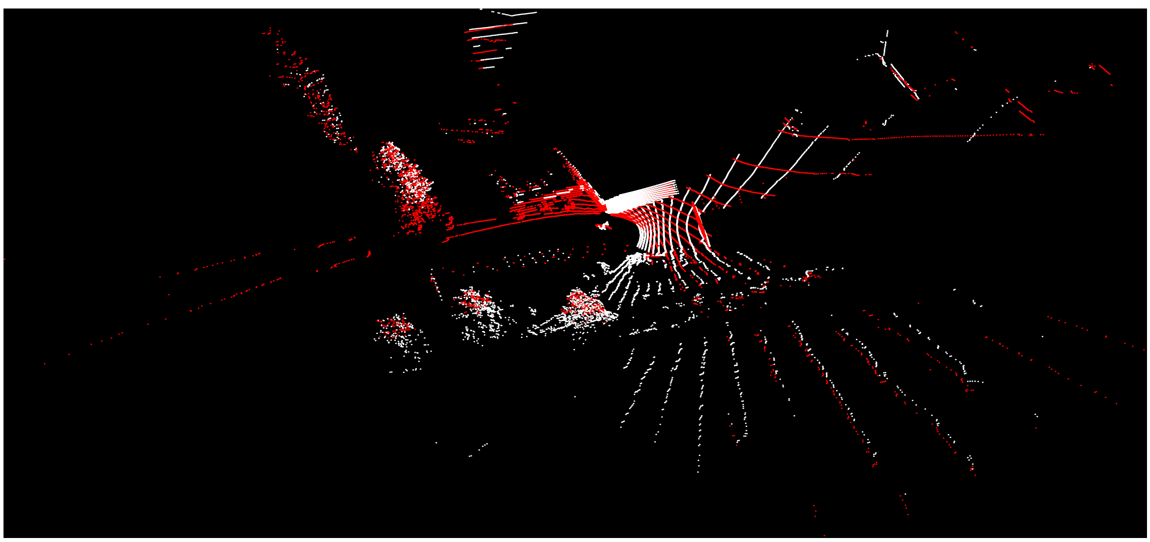

Fig. 8. Calibrated point clouds when the parameters shown in the Table 3 are used. The scene is the same as in Fig. 7.

Table 4
Obtained time-offsets.

-	IMU/GNSS	IMU/Right LiDAR	IMU/Left LiDAR	Left LiDAR/Right LiDAR
l (s)	0.0	0.1	0.0	0.0

for the point cloud-based and motion-based methods. Fig. 9 shows two examples of GNSS trajectories used in the point cloud-based calibration. Whereas Fig. 10 shows the angular velocities of the IMU and the LiDARs. These are used to calculate time-offsets that are shown in Table 4. Based on the results presented in Table 4, time offsets of 0 seconds are used because the LiDARs are similar and the difference in the right LiDAR is likely due to a noisy signal.

Table 5 shows the results when the point cloud-based and motion-based methods are used. In the point cloud-based method, a total of 5 different trajectories are used with different movements, and the translation of the z-axis is improved by using three of them where the tractor movement was slow.

A possible approach to verify the estimated parameters between the GNSS/IMU and the LiDARs is to determine the extrinsic parameters between the LiDAR sensors by utilizing results from Table 5. Hence, estimating the extrinsic parameters between the LiDAR sensors, the result should be approximately the same as shown in Section 3.1.2. Using this approach, the results shown in Table 6 are obtained.

3.3. Extrinsic calibration results between LiDAR and camera

The sample results from the extrinsic parameter calibration between the camera and the right LiDAR, as well as between the camera and the left LiDAR, can be seen in Fig. 11. Figure shows how the LiDAR scan lines from both the left LiDAR and the right LiDAR project onto the image plane when using the estimated parameter values shown in Table 7. This validates the mapping between sensor frames.

Again, the LiDAR-to-LiDAR transformation can be calculated by utilizing the above results between the camera and the LiDARs. Table 8 shows the LiDAR-to-LiDAR extrinsic parameters when the extrinsic parameters between the camera and LiDARs are utilized.

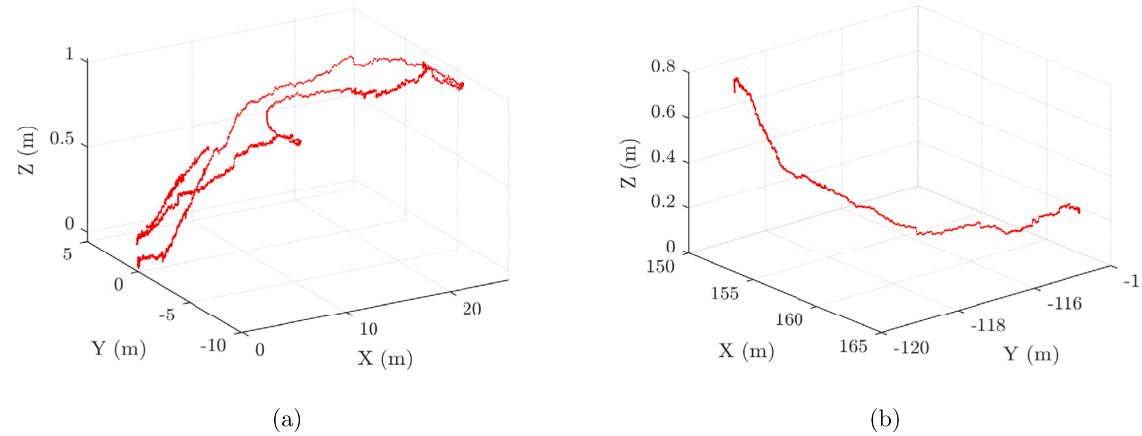

Fig. 9. (a) and (b) show two sample GNSS trajectories used in point cloud-based calibration.

Table 5
Extrinsic parameters obtained between the GNSS/IMU and the right LiDAR as well as between the GNSS/IMU and the left LiDAR. The results are obtained when the point cloud-based and motion-based methods are used.

Parameter	Right value point cloud	Left Value point cloud	Right Value motion	Left Value motion
t_x (m)	0.93	0.98	0.83	0.94
t_y (m)	-0.63	0.66	-0.65	0.64
t_z (m)	-0.15	-0.17	-0.42	-0.33
ψ (°)	-14.075	14.91	-13.15	15.15
θ (°)	19.37	16.59	18.84	16.03
ϕ (°)	1.92	-1.31	1.74	-2.59

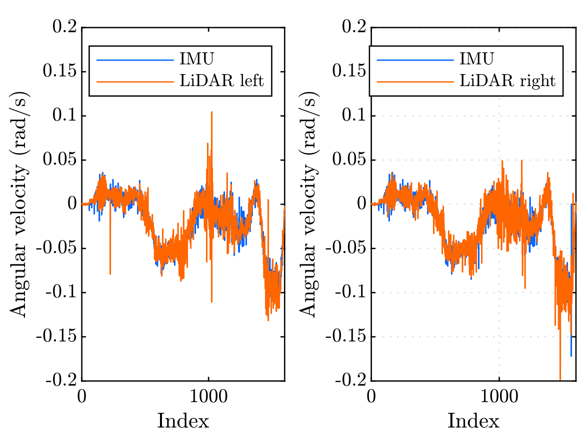

Fig. 10. Angular velocities of the IMU, left LiDAR, and right LiDAR.

Table 6
Extrinsic parameters obtained between LiDAR sensors using the results from this section. The Value Point cloud column corresponds to the point cloud-based method. The Value motion column corresponds to the motion-based method.

Parameter	Value Point cloud	Value Motion
t_x (m)	-0.37	-0.41
t_y (m)	-1.23	-1.21
t_z (m)	-0.11	-0.26
ψ (°)	-27.20	-26.55
θ (°)	5.32	5.77
ϕ (°)	11.07	11.62

Table 7
Extrinsic parameters obtained between the camera and the right LiDAR as well as between the camera and the left LiDAR. The right value and left value columns correspond to the values obtained between the camera and the right LiDAR and the camera and the left LiDAR, respectively.

Parameter	Right value	Left Value
t_x (m)	0.75	-0.61
t_y (m)	-0.10	-0.10
t_z (m)	-0.08	-0.07
ψ (°)	31.45	162.44
θ (°)	-75.67	-74.41
ϕ (°)	64.44	-77.08

Table 8
Extrinsic parameters obtained between the LiDAR sensors by utilizing results between camera and LiDAR calibration.

Parameter	Value
t_x (m)	-0.36
t_y (m)	-1.32
t_z (m)	-0.13
ψ (°)	-26.57
θ (°)	5.04
ϕ (°)	10.93

4. Discussion

The simulation environment was created and used to test the functionality of the plane-based calibration approach. The simulation results from Section 3.1.1 show that the estimated parameter values and the ground truth parameter values are close to the same. The absolute error in rotation is in the range between 0.044–0.066° and the error in translation is in the range between 0.0027–0.013. This indicates that the optimization method is able to determine correct parameter values in simulation. In Section 3.1.2 the results between the LiDAR sensors were shown when plane-based calibration was applied in the real calibration case. From Fig. 7 it can be seen that the method is also able to calibrate point clouds in real test case. The results from the real calibration case as well as from the simulation case are accordant with each other.

Fig. 11. Detected checkerboard from the right LiDAR and the left LiDAR point clouds projected onto the image plane when parameters available in Table 7 are used.

Despite the fact that the motion-based calibration method was primarily designed for extrinsic calibration between the GNSS/IMU unit and the LiDAR, it was also directly experimented in the case of LiDAR-to-LiDAR calibration to illustrate its relevance for various sensor types. The results from this were shown in Section 3.1.3. If comparing the obtained motion-based results with the plane-based approach, it can be seen that the biggest difference is in the z translation and the roll angle.

The extrinsic parameters were also calibrated between the GNSS/IMU unit and the LiDARs. For this calibration case, two calibration methods were investigated. These results were shown in section 3.2. The results indicate that the methods can find similar rotation parameters, but in translation there are differences, especially in the z-axis. This indicates that the point cloud-based method is able to give more accurate results.

The extrinsic calibration of parameters was also carried out between the camera and LiDARs. These results were shown in section 3.3. For this, the checkerboard approach was selected. The results suggest that the calibration was successful, the detected checkerboard from the LiDAR point cloud projects well onto the image plane as well as grounded on the fact that the obtained extrinsic parameters between the LiDARs are close to the same in Tables 2 and 8.

Table 9 compiles the extrinsic calibration results between the LIDAR sensors obtained using different calibration methods from Tables 2, 6 and 8 that were already presented in the result section into one table to enable easier comparison. As can be seen from the table, the results are generally consistent with each other. This further validates that the different methods used are capable of giving the correct results.

The results from the simulation and the real tests indicate that the plane-based approach is suitable for a structured man-made environment. The same is also noticed in previous studies that use planar structures during the calibration process [10]. This is also to some extent a limiting factor for fully automatic calibration in arbitrary environments. For instance, it is not possible for forestry machines working in the forest to exploit planar structures. However, for agricultural machines, this is not a very limiting factor because agricultural environments typically contain at least the buildings where the machines are kept.

Regarding the point-cloud-based extrinsic calibration between the LiDARs and the GNSS/IMU unit, the main assumption was that the GNSS/IMU unit could provide accurate estimates of the pose. If this assumption is not true, the method will not work. This kind of scenario would be possible, for example, in a full forest environment where RTK-GNSS positioning is not a reliable method [32]. The method developed in this study used a cylinder-shaped object, which means that the method is not completely human-free at the moment. However, the underlying optimization method can be extended to different kinds of features found in the environment.

Table 9
Summary of cross-validation results already shown in the result section. The plane column corresponds to the plane-based LiDAR-to-LiDAR calibration. The point cloud and the motion columns correspond to LiDAR-to-LiDAR extrinsic parameters obtained using the results between the GNSS/IMU and the LiDARs. The checkerboard column corresponds to the LiDAR-to-LiDAR extrinsic parameters obtained using results between the camera and the LiDARs.

Parameter	Plane	Point cloud	Motion	Checkerboard
t_x (m)	-0.35	-0.37	-0.41	-0.36
t_y (m)	-1.30	-1.23	-1.21	-1.32
t_z (m)	-0.14	-0.11	-0.26	-0.13
ψ (°)	-26.74	-27.20	-26.55	-26.57
θ (°)	5.05	5.32	5.77	5.04
ϕ (°)	11.02	11.07	11.62	10.93

Regarding the motion-based calibration, the main challenge for accurate and fully automatic calibration is to obtain enough accurate motion estimates for LiDAR odometry. The LiDAR-only odometry can be inaccurate, especially if the tractor's movement is desired to vary in z-height and in pitch and roll angles. If the vehicle motion profile is primarily planar, the z-axis translation is unobservable. Because of that the motion-only method can not determine the z-axis translation reliably. This is also a major separating aspect between traditional robotic arm hand-eye calibration and autonomous vehicle motion-based calibration. This is a thing often noticed in the previous literature working with motion-based calibration in autonomous vehicle applications [33] [18] [17]. The main advantage of the motion-based method is that it can be used to estimate extrinsic parameters between different sensors, as also shown in this paper. This can be utilized as initial estimates for more accurate methods as done in this paper. Regarding the parameters, the average standard deviation between the translational parameters between the LiDARs is 0.0491 m and for rotation it is 0.3189°. Furthermore, it can be said that the parameters that can be considered the most reliable are the plane-based calibration between LiDARs and the point cloud-based calibration between LiDAR and GNSS/IMU. Future work includes the online implementation of the methods.

5. Conclusion

In this study, extrinsic parameter calibration methods were developed, implemented, and tested between different sensors. The main contribution of this paper was to consistently study extrinsic calibration algorithms in the case of the robot tractor in the agricultural environment context. The methods used planes extracted from the environment, point clouds, sensor motion, or traditional chessboard in the calibration process depending on the sensors under calibration. The results indicated that consistent extrinsic parameter results can be obtained using the methods shown in this paper. This was validated using the simulation environment, visual inspection of the results, and by estimating LiDAR-to-LiDAR extrinsic parameters with different methods presented in this paper.

CRediT authorship contribution statement

Jere Knuutinen: Writing – original draft, Visualization, Validation, Software, Methodology, Investigation, Formal analysis, Data curation, Conceptualization. **Juha Backman:** Writing – review & editing, Supervision, Resources, Project administration, Methodology, Funding acquisition, Conceptualization. **Raimo Linkolehto:** Resources, Investigation, Data curation. **Arto Visala:** Writing – review & editing, Supervision, Investigation, Conceptualization.

Declaration of competing interest

The authors declare that they have no known competing financial interests or personal relationships that could have appeared to influence the work reported in this paper.

Acknowledgement

This research was conducted by Aalto University and Natural Resources Institute Finland (LUKE) as part of the European Union's Horizon 2020 research and innovation programme under grant agreement No 101017111 (FlexiGroBots project).

A part of the work was also carried out in the AGRIForward project, which is part of the Forward'27 ecosystem programme by the Ponsse Group, funded by Business Finland's Veturi funding and supported by several Finnish companies.

Data availability

Data will be made available on request.

References

[1] Agriculture and food, https://www.worldbank.org/en/topic/agriculture/overview. (Accessed 3 May 2023).
[2] J. Kaivosoja, Role of Spatial Data Uncertainty in Executions of Precision Farming Operations, Aalto University, 2019, https://aaltodoc.aalto.fi/handle/123456789/41363.
[3] Y. Bai, B. Zhang, N. Xu, J. Zhou, J. Shi, Z. Diao, Vision-based navigation and guidance for agricultural autonomous vehicles and robots: a review, Comput. Electron. Agric. 205 (2023) 107584, https://doi.org/10.1016/j.compag.2022.107584.
[4] A. Bechar, C. Vigneault, Agricultural robots for field operations: concepts and components, Biosyst. Eng. 149 (2016) 94–111, https://doi.org/10.1016/j.biosystemseng.2016.06.014.
[5] J. Kim, C. Kim, H.J. Kim, Robust extrinsic calibration for arbitrarily configured dual 3d lidars using a single planar board, in: 2020 20th International Conference on Control, Automation and Systems (ICCAS), 2020, pp. 576–580.
[6] L. Zhou, Z. Li, M. Kaess, Automatic extrinsic calibration of a camera and a 3d lidar using line and plane correspondences, in: 2018 IEEE/RSJ International Conference on Intelligent Robots and Systems (IROS), 2018, pp. 5562–5569.
[7] J. Beltrán, C. Guindel, A. de la Escalera, F. García, Automatic extrinsic calibration method for lidar and camera sensor setups, IEEE Trans. Intell. Transp. Syst. 23 (10) (2022) 17677–17689, https://doi.org/10.1109/TITS.2022.3155228.
[8] H. Lee, W. Chung, Extrinsic calibration of multiple 3d lidar sensors by the use of planar objects, Sensors 22 (19) (2022), https://doi.org/10.3390/s22197234.
[9] J. Jiao, Q. Liao, Y. Zhu, T. Liu, Y. Yu, R. Fan, L. Wang, M. Liu, A novel dual-lidar calibration algorithm using planar surfaces, in: 2019 IEEE Intelligent Vehicles Symposium (IV), 2019, pp. 1499–1504.
[10] D.-H. Kim, G.-W. Kim, Automatic multiple lidar calibration based on the plane features of structured environments, IEEE Access 9 (2021) 84387–84402, https://doi.org/10.1109/ACCESS.2021.3087266.
[11] R. Tsai, R. Lenz, Real time versatile robotics hand/eye calibration using 3d machine vision, in: Proceedings, 1988 IEEE International Conference on Robotics and Automation, vol. 1, 1988, pp. 554–561.
[12] D. Wenberg, A. Ray, R. Sander, Lidar-lidar hand-eye calibration via optimization on se(3), https://doi.org/10.13140/RG.2.2.25464.67840, 01 2021.
[13] J. Jiao, Y. Yu, Q. Liao, H. Ye, R. Fan, M. Liu, Automatic calibration of multiple 3d lidars in urban environments, in: 2019 IEEE/RSJ International Conference on Intelligent Robots and Systems (IROS), 2019, pp. 15–20.
[14] R. Ishikawa, T. Oishi, K. Ikeuchi, Lidar and camera calibration using motion estimated by sensor fusion odometry, CoRR, arXiv:1804.05178, 2018.
[15] R. Horaud, F. Dornaika, Hand-eye calibration, Int. J. Robot. Res. 14 (3) (1995) 195–210, https://doi.org/10.1177/027836499501400301.
[16] A. Geiger, P. Lenz, C. Stiller, R. Urtasun, Vision meets robotics: the kitti dataset, Int. J. Robot. Res. (2013).
[17] X. Nie, J. Gong, J. Cheng, X. Tang, Y. Zhang, Two-step self-calibration of lidar-gps/imu based on hand-eye method, Symmetry 15 (2) (2023), https://doi.org/10.3390/sym15020254.
[18] X. Yuwen, L. Chen, F. Yan, H. Zhang, J. Tang, B. Tian, Y. Ai, Improved vehicle lidar calibration with trajectory-based hand-eye method, IEEE Trans. Intell. Transp. Syst. 23 (1) (2022) 215–224, https://doi.org/10.1109/TITS.2020.3009674.
[19] J. Pi, G. Yan, C. Wang, X. Cai, B. Shi, An extrinsic calibration method between lidar and gnss/ins for autonomous driving, in: 2024 IEEE International Conference on Robotics and Automation (ICRA), 2024, pp. 14520–14526.
[20] W. Yang, Y. Bu, D. Li, W. Xu, Mcsgcalib: multi-constraint-based extrinsic calibration of solid-state lidar and gnss/ins for autonomous vehicles, IEEE Trans. Intell. Transp. Syst. 25 (11) (2024) 18791–18804, https://doi.org/10.1109/TITS.2024.3428319.
[21] C. Xia, Y. Shen, T. Zhang, S. Zhang, Y. Huo, S. Chen, N. Zheng, Robust extrinsic parameter calibration of 3d lidar using Lie algebras, in: 2019 IEEE Intelligent Vehicles Symposium (IV), 2019, pp. 1775–1781.
[22] J. Backman, R. Linkolehto, M. Lemsalu, J. Kaivosoja, Building a robot tractor using commercial components and widely used standards, IFAC-PapersOnLine 55 (32) (2022) 6–11, https://doi.org/10.1016/j.ifacol.2022.11.106.
[23] Region growing segmentation, https://pcl.readthedocs.io/projects/tutorials/en/latest/region_growing_segmentation.html. (Accessed 2 May 2023).
[24] K. Favre, M. Pressigout, E. Marchand, L. Morin, A plane-based approach for indoor point clouds registration, in: 2020 25th International Conference on Pattern Recognition (ICPR), 2021, pp. 7072–7079.
[25] Y. Taguchi, Y.-D. Jian, S. Ramalingam, C. Feng, Point-plane slam for hand-held 3d sensors, in: 2013 IEEE International Conference on Robotics and Automation, 2013, pp. 5182–5189.
[26] Z. Zhou, Y. Qiao, A. Yang, A robust point cloud registration method for structured scenes based on plane elements using global information, in: 2022 5th International Symposium on Autonomous Systems (ISAS), 2022, pp. 1–6.
[27] T. Välimäki, B. Garigipati, R. Ghabcheloo, Motion-based extrinsic sensor-to-sensor calibration: effect of reference frame selection for new and existing methods, Sensors 23 (7) (2023), https://doi.org/10.3390/s23073740, https://www.mdpi.com/1424-8220/23/7/3740.
[28] K. Chen, B.T. Lopez, A.-a. Agha-mohammadi, A. Mehta, Direct lidar odometry: fast localization with dense point clouds, IEEE Robot. Autom. Lett. 7 (2) (2022) 2000–2007, https://doi.org/10.1109/LRA.2022.3142739.
[29] N. Boumal, B. Mishra, P.-A. Absil, R. Sepulchre, Manopt, a Matlab toolbox for optimization on manifolds, J. Mach. Learn. Res. 15 (42) (2014) 1455–1459, https://www.manopt.org.
[30] MathWorks, Lidar toolbox documentation, https://www.mathworks.com/help/lidar/index.html?s_tid=CRUX_lftnav. (Accessed 28 April 2025).
[31] Dataspeed Inc, velodyne_simulator, https://bitbucket.org/DataspeedInc/velodyne_simulator/src/master/. (Accessed 7 May 2023).
[32] T. Badar, I. Ouattara, J. Backman, A. Visala, Estimation of 3d form of the path for autonomous driving in terrain*, IFAC-PapersOnLine 56 (2) (2023) 4916–4921, https://doi.org/10.1016/j.ifacol.2023.10.1264, 22nd IFAC World Congress.
[33] M. Pekkanen, Motion-based extrinsic parameter calibration of a robot's multisensor system, Master's thesis, Aalto University, School of Electrical Engineering, 2018.